FLUCTUATING HYDRODYNAMIC METHODS FOR FLUID-STRUCTURE INTERACTIONS IN CONFINED CHANNEL GEOMETRIES

YAOHONG WANG * AND PAUL J. ATZBERGER †

Abstract. We develop computational methods for the study of fluid-structure interactions subject to thermal fluctuations when confined within a channel. Our methods take into account the hydrodynamic coupling and diffusivity of microstructures when influenced by their proximity to no-slip walls. We develop stochastic numerical methods subject to no-slip boundary conditions using a staggered finite volume discretization. We show that by imposing an exact fluctuation-dissipation condition to discretize the stochastic driving fields combined with using an exact projection method to enforce incompressibility is sufficient to ensure results consistent with statistical mechanics. We demonstrate our methods by investigating how the proximity of ellipsoidal colloids to the channel wall effects their active hydrodynamic responses and passive diffusivity. We also study the collective dynamics of a large number of particles by considering the intermediate scattering functions for the relaxation of density fluctuations. We expect our introduced stochastic computational methods to be applicable broadly to applications in which confinement effects play an important role in the dynamics of microstructures subject to hydrodynamic coupling and thermal fluctuations.

Key words. Fluctuating Hydrodynamics, Stochastic Eulerian Lagrangian Method, Immersed Boundary Method, Ellipsoidal Colloids, Mobility, Nanochannel.

Last update to manuscript was on September 11, 2013; 2:13pm.

1. Introduction.

Hydrodynamic coupling and collective diffusivity can be significantly augmented by the proximity of microstructures to a surface. This is often relevant to transport phenomena in many applications, such as the electrophoresis of macromolecules and colloids in capillaries [17, 18, 33, 24], processing of emulsions and polymers in microfluidic devices [22, 34, 32, 31, 8], or the behaviors of active suspensions such as swimming microorganisms near surfaces [14, 36]. We develop stochastic computational methods to capture confinement effects of microstructures within channel geometries with no-slip walls. Our approach is based on the Stochastic Eulerian-Lagrangian Method (SELM) which provides tractable ways to incorporate thermal fluctuations into approximate descriptions of the hydrodynamic coupling between microstructures [4]. In SELM, fluctuating hydrodynamic equations similar to those introduced by Landau and Lifshitz [21] are coupled and exchange momentum with microstructure conservation equations. The SELM framework provides criteria to ensure that the continuum stochastic description and related stochastic discretizations yield results consistent with statistical mechanics [4]. Related computational methods for fluctuating hydrodynamics have also been introduced in [5, 7, 6, 15, 12].

We present the SELM approach for the channel geometry in Section 2. We develop stochastic numerical methods using a staggered finite volume discretization for the fluid velocity and pressure in Section 3. To obtain a consistent discretization of the stochastic driving fields as in [5, 4], we impose an exact fluctuation-dissipation balance on our stochastic numerical methods taking into account the augmented dissipative properties of the discrete operators relative to their continuum differential counterparts in Section 3.1. We show that our numerical fluctuation-dissipation balance principle combined with using an exact projection method for the incompressibility is sufficient to ensure results consistent with statistical mechanics in Section 3.2. In practice, a significant challenge is to generate efficiently the stochastic driving fields with the required covariance structure obtained from the

*University of California, Department of Mathematics

†University of California, Department of Mathematics , Santa Barbara, CA 93106; e-mail: atzberg@math.ucsb.edu; phone: 805-893-3239; Work supported by W.M. Keck Foundation, DOE CM4, and NSF CAREER Grant DMS-0956210.

fluctuation-dissipation balance condition. We show how a method with cost $O(N\log(N))$ can be developed for our discretization based on FFTs to generate efficiently the driving fields in the presence of the no-slip walls in Section 3.3. We validate the computational methods in Section 4 by performing studies for the stochastic field generation in Section 4.1 and for the Brownian motion of a particle diffusing in a harmonic potential in Section 4.2. As a demonstration of our computational methods we consider ellipsoidal particles within a channel and investigate the effects of confinement on both active hydrodynamic responses and passive diffusivity in Section 5. We first compare our computational model of ellipsoidal particles to those of analytic results for the translational and rotational mobility in Section 5.1. We then investigate how the proximity of a particle to a wall within the channel effects the mobility of the ellipsoidal colloids in response to active forces or torques in Section 5.2. We then demonstrate through stochastic simulations that our fluctuating hydrodynamic methods capture the role of proximity to the no-slip walls as manifested in the empirical diffusivity of particles. We show our stochastic methods yield diffusivities in close agreement in accordance with the Stokes-Einstein relations with the predictions from the active mobility studies in Section 5.4. We then make comparisons to conventional Langevin dynamics in Section 5.5. We study the collective dynamics of a large number of colloidal particles within the channel and their density relaxations. We find our fluctuating hydrodynamics approach yields results having significant differences with simulations performed with conventional Langevin dynamics that neglects the hydrodynamic coupling. We conclude by investigating these differences by considering the intermediate scattering functions of the density relaxations. Overall, we expect our introduced stochastic computational methods to be applicable broadly to problems involving confinement effects of microstructures subject to hydrodynamic coupling and thermal fluctuations.

2. Fluid-Structure Interactions Subject to Thermal Fluctuations. Our description of the fluid-structure interactions subject to thermal fluctuations is based on the Stochastic Eulerian Lagrangian Method (SELM) [4]. In SELM the microstructures exchange momentum with a fluctuating fluid to account simultaneously for hydrodynamic coupling and thermal fluctuations. SELM provides a way to incorporate thermal fluctuations into widely used approaches for approximating the fluid-structure interactions [4]. We extend the SELM approach to account for no-slip walls when the microstructures and fluid are confined within a channel geometry. For the microstructure dynamics, we use

$$\frac{d\mathbf{X}}{dt} = \mathbf{v} \tag{2.1}$$

$$m\frac{d\mathbf{v}}{dt} = -\Upsilon(\mathbf{v} - \Gamma\mathbf{u}) - \nabla_X \Phi[X] + \mathbf{F}_{thm}. \tag{2.2}$$

These are coupled to the incompressible fluctuating hydrodynamic equations

$$\rho\frac{\partial \mathbf{u}}{\partial t} = \mu\Delta\mathbf{u} + \Lambda[\Upsilon(\mathbf{v} - \Gamma\mathbf{u})] - \nabla p + \mathbf{f}_{thm} \tag{2.3}$$

$$\nabla\cdot\mathbf{u} = 0. \tag{2.4}$$

We consider these on the domain $\Omega = [0, L_x]\times[0, L_y]\times[0, L_z]$ subject to the no-slip boundary condition

$$\mathbf{u}(\mathbf{x}, t) = 0, \qquad \mathbf{x}\in\partial\Omega^{(z)}. \tag{2.5}$$

The $\Omega^{(z)}$ denotes the part of the boundary when $z = 0$ or $z = L_z$. The $\mathbf{X}$ denotes the collective vector of all of the degrees of freedom of the microstructure, the $\mathbf{v}$ the microstructure velocity, and m the microstructure excess mass [4, 3]. The fluid velocity is denoted by $\mathbf{u}$, the fluid density by ρ, and the dynamic viscosity by μ. The pressure acts as a Lagrange multiplier to enforce the incompressibility constraint given in equation 2.4.

The operators Γ and Λ serve to couple the microstructure and fluid dynamics. The Γ operator serves to provide a local reference velocity from the fluid against which the

microstructure velocity is compared. The term $-\Upsilon(\mathbf{v} - \Gamma\mathbf{u})$ acts as an effective drag force on the microstructure when its velocity differs from that of the surrounding fluid. The Υ is assumed to be a positive-definite operator. The Λ operator is introduced to account for the drag of a moving particle's force equal-and-opposite effect on the fluid. The Λ operator converts a microstructure force into a corresponding force density in the fluid equations in equation 2.3. A particularly important property to obtain consistent results in the mechanics is that the coupling operators satisfy an adjoint condition $\Lambda = \Gamma^T$, [4, 3, 27].

To account for thermal fluctuations, we let $\mathbf{F}_{thm}$ and $\mathbf{f}_{thm}$ be Gaussian random fields that are δ-correlated in time and have zero mean [16, 25]. We determine the spatial covariance using the fluctuation-dissipation principle of statistical mechanics [29, 4]

$$\langle \mathbf{f}_{\text{thm}}(s)\mathbf{f}^T_{\text{thm}}(t)\rangle = -\left(2k_BT\right)\left(\Delta - \Lambda\Upsilon\Gamma\right)\delta(t-s) \tag{2.6}$$

$$\langle \mathbf{F}_{\text{thm}}(s)\mathbf{F}^T_{\text{thm}}(t)\rangle = \left(2k_BT\right)\Upsilon\,\delta(t-s) \tag{2.7}$$

$$\langle \mathbf{f}_{\text{thm}}(s)\mathbf{F}^T_{\text{thm}}(t)\rangle = -\left(2k_BT\right)\Lambda\Upsilon\,\delta(t-s). \tag{2.8}$$

The adjoint condition $\Lambda = \Gamma^T$ has been shown to play an important role when introducing the stochastic driving fields [4]. Throughout our discussion, our stochastic differential equations should be given the Ito interpretation in stochastic calculus [25, 16].

A widely used approximation to obtain a tractable description of the fluid-structure interactions is the *Immersed Boundary Method* [27]. This corresponds to the specific choice of coupling operators

$$\Gamma\mathbf{u} = \int_\Omega \eta\left(\mathbf{y} - \mathbf{X}(t)\right)\mathbf{u}(\mathbf{y},t)d\mathbf{y} \tag{2.9}$$

$$\Lambda\mathbf{F} = \eta\left(\mathbf{x} - \mathbf{X}(t)\right)\mathbf{F}. \tag{2.10}$$

The kernel functions $\eta(\mathbf{z})$ are chosen to be the Peskin δ-Function developed in [27]. The Peskin δ-Function has important numerical properties that ensure to a good approximation that there is translational invariance of the coupling despite the breaking of this symmetry by the discretization lattice of the fluid [5, 27, 30]. A kernal with finite support is chosen instead of a Dirac δ-Function to ensure a model in which the mobility of even individual point particles have a finite effective hydrodynamic radius within the fluid [5]. Since other choices for the fluid-structure coupling can also be useful, we only make use of the generic properties of Γ, Λ throughout the mathematical discussions. For coupling the fluid and microstructure we use the Stokes drag

$$\Upsilon = 6\pi\mu R, \tag{2.11}$$

where R is a length-scale which we take to be comparable to the support of the kernel function $\eta(\mathbf{x})$. Provided Υ is sufficiently large, the precise value does not play a particularly central role in the dynamics [3, 4].

3. Semidiscretization : Staggered Finite Volume Method. We discretize the system using a finite volume approximation on a staggered grid for the velocity and pressure. The velocity components are represent at the cell faces and the pressure at the cell centers, see Figure 3.1. A particular advantage of the staggered grid discretization is that the mass transport can be modeled naturally between the cells using fluxes based on the velocity at the cell faces. This is also useful in approximating the divergence-free incompressibility constraint since it arises in the continuum fluid mechanics from the continuity equations and the requirement that a uniform mass density remain constant under the fluid flow. Using this interpretation in the finite volume setting yields a constraint on the discrete velocity field expressed in terms of a discrete divergence operator which can be imposed exactly using the cell centered pressure and its discrete gradient. The finite volume formulation provides a finite difference method with a set of discrete operators playing roles very similar to their continuum differential counterparts. We shall show in the stochastic setting these features have important implications for the statistical mechanics of our stochastic numerical

methods. Related finite volume schemes for fluctuating hydrodynamics have been introduced in [6, 5, 12].

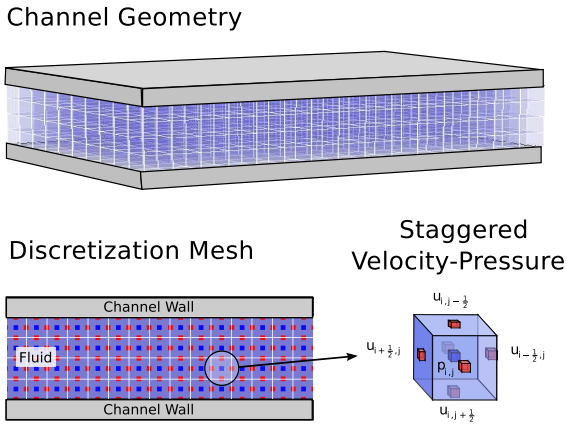

FIG. 3.1. *Channel Geometry and Staggered Finite Volume Discretization. The fluctuating hydrodynamic equations are approximated using a staggered finite volume discretization. The velocity is represented on the cell faces and the pressure is represented at the cell centers. An important feature of the discretization is the ability to approximate the incompressibility constraint using an exact projection method.*

We use for our discretization a computational domain decomposed into $N_x \times N_y \times N_z$ cells indexed by $\mathbf{m} = (i, j, k)$. We decompose the fluid velocity $\mathbf{u} = (u^{(1)}, u^{(2)}, u^{(3)}) = (u, v, w)$ into its Cartesian components at each cell face. We index the fluid velocity in the x-direction by half indices $u_{i\pm 1/2,j,k}$, and similarly for the other directions. The pressure p is defined at the cell centers and indexed by (i, j, k) as $p_{i,j,k}$. The no-slip boundary conditions are imposed by requiring in the z-direction $w_{i,j,-1/2} = w_{i,j,N_z-1/2} = 0$. The x-direction and y-direction are treated as periodic with the condition $u_{i,j,-1/2} = u_{i,j,N_z+1/2}$, $v_{i,j,-1/2} = v_{i,j,N_y+1/2}$. To simplify the notation, we shall often use the vector-index notation $\mathbf{u_I}$, $p_\mathbf{I}$ with $\mathbf{I} = (i, j, k)$. We let Ω_c denote the collection of *cell indices* within the interior of the domain and let $\partial\Omega_c$ denote the cell indices on the boundary. Similarly, we let Ω_f denote the collection of *face indices* within the interior of the domain and let $\partial\Omega_f$ denote the indices on the boundary.

We use the finite volume interpretation to define the discrete divergence operator $\mathcal{D}$ by

$$(\mathcal{D} \cdot \mathbf{u})_\mathbf{m} = \frac{1}{\Delta x} \sum_{d=1}^{3} \left(u^{(d)}_{\mathbf{m}+\frac{1}{2}\mathbf{e}_d} - u^{(d)}_{\mathbf{m}-\frac{1}{2}\mathbf{e}_d} \right) \tag{3.1}$$

where $\mathbf{e}_d$ is the standard basis vector in the d-direction. We define the discrete gradient operator $\mathcal{G}$ using the negative adjoint of the discrete divergence operator $\mathcal{G} = -\mathcal{D}^T$ which yields

$$(\mathcal{G}p)_{\mathbf{m}\pm\frac{1}{2}\mathbf{e}_d} = \pm\frac{1}{\Delta x} \left(p_{\mathbf{m}\pm\mathbf{e}_d} - p_\mathbf{m} \right). \tag{3.2}$$

We define the face centered Laplacian $\mathcal{L}_f$ as

$$(\mathcal{L}_f \mathbf{u})_{\mathbf{m}\pm\frac{1}{2}\mathbf{e}_d} = \frac{1}{\Delta x^2} \sum_{a=1}^{3} \left(\mathbf{u}_{\mathbf{m}\pm\frac{1}{2}\mathbf{e}_d+\mathbf{e}_a} - 2\mathbf{u}_{\mathbf{m}\pm\frac{1}{2}\mathbf{e}_d} + \mathbf{u}_{\mathbf{m}\pm\frac{1}{2}\mathbf{e}_d-\mathbf{e}_a} \right). \tag{3.3}$$

We define a cell centered Laplacian $\mathcal{L}_c$ using the discrete divergence and gradient operators

$$(\mathcal{L}_c p)_\mathbf{m} = (\mathcal{D} \cdot \mathcal{G}p)_\mathbf{m} = \frac{1}{\Delta x^2} \sum_{d=1}^{3} \left(p_{\mathbf{m}+\frac{1}{2}\mathbf{e}_d} - 2p_\mathbf{m} + p_{\mathbf{m}-\frac{1}{2}\mathbf{e}_d} \right). \tag{3.4}$$

We use our discrete operators to approximate the equations 2.1– 2.4 to obtain the semidiscretization

$$\rho\frac{\partial \mathbf{u}}{\partial t} = \mu\mathcal{L}_f\mathbf{u} + \Lambda[\Upsilon(\mathbf{v} - \Gamma\mathbf{u})] - \mathcal{G}p + \mathbf{f}_{thm} \tag{3.5}$$

$$\mathcal{D}\cdot\mathbf{u} = 0 \tag{3.6}$$

$$m\frac{d\mathbf{v}}{dt} = -\Upsilon(\mathbf{v} - \Gamma\mathbf{u}) - \nabla_X\Phi[X] + \mathbf{F}_{thm} \tag{3.7}$$

$$\frac{d\mathbf{X}}{dt} = \mathbf{v}. \tag{3.8}$$

These are subject to the boundary conditions

$$\mathbf{u}_\mathbf{m} = 0, \qquad \mathbf{m} \in \partial\Omega_f \tag{3.9}$$

$$(\mathcal{G}p)_\mathbf{m}\cdot\mathbf{n} = 0, \qquad \mathbf{m} \in \partial\Omega_f. \tag{3.10}$$

Using the finite volume interpretation of our discretized system we associate the energy

$$E\left[\mathbf{u},\mathbf{v},\mathbf{X}\right] = \sum_\mathbf{m}\frac{1}{2}\rho|\mathbf{u}_\mathbf{m}|^2\Delta\mathbf{x}^3_\mathbf{m} + \frac{1}{2}m|\mathbf{v}|^2 + \Phi\left[\mathbf{X}\right]. \tag{3.11}$$

The $\Delta\mathbf{x}^3_\mathbf{m}$ denotes the volume of the cell with index $\mathbf{m}$. We integrate numerically in time the equations 3.5– 3.8 using the Euler-Maruyama method [20].

An important consideration for the semidiscretized system is that the discrete operators have different dissipative properties than their continuum differential counterparts. It becomes important in the discrete stochastic setting to take this into account in the choice of the stochastic driving fields $\mathbf{F}_{thm}$ and $\mathbf{f}_{thm}$ to ensure appropriate thermal fluctuations consistent with statistical mechanics [4, 5].

3.1. Stochastic Driving Fields for the Discretization. To account for the thermal fluctuations in the discrete setting we must approximate the stochastic driving fields in equations 2.1– 2.3. We must also take into account in the discrete setting the role of the incompressibility constraint. Another important consideration is that the dissipative properties of the discrete operators are often significantly different than their continuum differential counterparts. The properties of the specific discretization and how constraints are handled have important implications for how fluctuations propagate through the degrees of freedom of the discretized system [4, 5].

We treat the incompressibility constraint by imposing exactly the discrete divergence-free condition 3.6 and using the projection method [9]. This approach allows for the semidiscretization in equations 3.5– 3.8 to be expressed as

$$\rho\frac{\partial \mathbf{u}}{\partial t} = \wp\left(\mu\mathcal{L}_f\mathbf{u} + \Lambda[\Upsilon(\mathbf{v} - \Gamma\mathbf{u})] + \mathbf{f}_{thm}\right) \tag{3.12}$$

$$m\frac{d\mathbf{v}}{dt} = -\Upsilon(\mathbf{v} - \Gamma\mathbf{u}) - \nabla_X\Phi[X] + \mathbf{F}_{thm} \tag{3.13}$$

$$\frac{d\mathbf{X}}{dt} = \mathbf{v}. \tag{3.14}$$

The projection operator $\wp$ is

$$\wp = \mathcal{I} - \mathcal{G}\mathcal{L}_c^{-1}\mathcal{D}\cdot \tag{3.15}$$

We approximate the stochastic driving fields by imposing on the discretization the following fluctuation-dissipation condition [29, 5, 4]

$$\langle\mathbf{F}\mathbf{F}^T\rangle = \mathbb{G} = -\mathbb{L}C - (\mathbb{L}C)^T. \tag{3.16}$$

The $\mathbf{F} = [\mathbf{f}_{thm}, \mathbf{F}_{thm}]$ represents the stochastic terms in the system of equations 3.5– 3.8. The $\mathbb{L}$ is the grand dissipative operator given by

$$\mathbb{L} = \begin{bmatrix} \rho^{-1}\mu\mathcal{L}_f - \rho^{-1}\Lambda\Upsilon\Gamma & \rho^{-1}\Lambda\Upsilon \\ m^{-1}\Upsilon\Gamma & -m^{-1}\Upsilon \end{bmatrix}. \tag{3.17}$$

An important part of our discretization method for the stochastic fields is the choice of covariance C we impose for the equilibrium fluctuations of the discrete system. We introduced an energy based on our finite volume interpretation in equation 3.11. Using the Gibbs-Boltzmann statistics associated with our discrete energy, we impose the covariance

$$C = k_B T \begin{bmatrix} \rho^{-1}\Delta\mathbf{x}_\mathbf{n}^{-3} & 0 \\ 0 & m^{-1} \end{bmatrix}. \tag{3.18}$$

Now that $\mathbb{L}$ and C are specified, our discrete fluctuation-dissipation condition given in equation 3.16 provides our approximation of the stochastic driving fields $\mathbf{F}$ through the covariance

$$\mathbb{G} = -2k_B T \begin{bmatrix} \rho^{-2}\Delta\mathbf{x}_\mathbf{n}^{-3}\mu\mathcal{L}_f - \rho^{-2}\Delta\mathbf{x}_\mathbf{n}^{-3}\Lambda\Upsilon\Gamma & m^{-1}\rho^{-1}\Lambda\Upsilon \\ m^{-1}\rho^{-1}\Delta\mathbf{x}_\mathbf{n}^{-3}\Upsilon\Gamma & m^{-2}\Upsilon \end{bmatrix}. \tag{3.19}$$

By using the fluctuation-dissipation condition 3.16 to discretize the stochastic driving fields, we have taken into account the properties of the specific choice of discretization and how this influences the propagation of fluctuations throughout the system [4, 5]. This approach drawing on insights from statistical mechanics also circumvents a number of potentially subtle issues in how directly to interpret and approximate the stochastic fluid equations which have solutions only in the generalized sense of distributions [4, 5].

We remark for the sake of our subsequent presentation and calculations that the precise form of the adjoint condition for Λ, Γ depends on the utilized representation of the operators and the inner-product. When representing the operators as standard matrices and using the standard matrix-vector inner product, the adjoint condition takes on the form $\Lambda^T = \Delta\mathbf{x}_\mathbf{n}^{-3}\Gamma$, hence the apparent asymmetric factor of $\Delta\mathbf{x}_\mathbf{n}^{-3}$ appearing in equations 3.19. Because of this interpretation, this in fact does not pose an issue in practice.

3.2. Statistical Mechanics of the Discretization subject to the Incompressibility Constraint. The stochastic driving fields were discretized without explicit consideration of the incompressibility constraint. We perform analysis to explore the implications of this constraint on the statistical mechanics of the stochastic dynamics. In our approach, the incompressibility is imposed each time-step using the Lagrange multiplier $\mathcal{G}p$ which is obtained from the discrete pressure p solving

$$\mathcal{L}_c p = \mathcal{D} \cdot [\Lambda[\Upsilon(\mathbf{v}^n - \Gamma\mathbf{u}^n)] + \mathbf{f}_{thm}^n] \tag{3.20}$$

$$(\mathcal{G}p)_\mathbf{m} \cdot \mathbf{n} = 0, \qquad \mathbf{m} \in \partial\Omega_f. \tag{3.21}$$

In practice to solve efficiently these equations, use Fast Fourier Transforms (FFTs) adapted to the channel geometry. We use standard FFTs in the periodic x and y-directions [11, 28]. To account for the Neumann boundary conditions in the z-direction, we use a Fast Cosine Transform (FCT) [28]. By substituting for the solution $\mathcal{G}p^n$ into equation 3.5 we obtain the same result as applying the projection operator given in equation 3.12. In this manner the fluctuating hydrodynamics satisfies exactly in the discrete setting the divergence-free incompressibility condition $\mathcal{D} \cdot \mathbf{u} = 0$.

Under the projected stochastic dynamics, we show invariance of the Gibbs-Boltzmann distribution

$$\Psi(\mathbf{u}, \mathbf{v}, \mathbf{X}) = \frac{1}{Z} \exp\left[-\frac{E[\mathbf{u}, \mathbf{v}, \mathbf{X}]}{k_B T}\right]. \tag{3.22}$$

The Z denotes the partition function. The Gibbs-Boltzmann distribution under the projected stochastic dynamics satisfies

$$\frac{\partial\Psi}{\partial t} = -\nabla \cdot \mathbf{J} \tag{3.23}$$

with probability flux on phase-space

$$\mathbf{J} = \begin{bmatrix} \rho^{-1}\mu\wp\mathcal{L}_f - \rho^{-1}\wp\Lambda\Upsilon\Gamma + \rho^{-1}\wp\Lambda\Upsilon \\ -m^{-1}\Upsilon + m^{-1}\Upsilon\Gamma - m^{-1}\nabla_{\mathbf{X}}\Phi \\ \mathbf{v} \end{bmatrix} \Psi - \frac{1}{2}(\nabla\cdot\overline{\mathbb{G}})\Psi - \frac{1}{2}\overline{\mathbb{G}}\nabla\Psi. \tag{3.24}$$

The stochastic driving field when subjected to the projection operator yields the term $\overline{\mathbf{F}} = \wp\mathbf{F}$. Hence the covariance for the stochastic driving field when subjected to the projection operator is given by $\overline{\mathbb{G}} = \wp\mathbb{G}\wp^T$. The divergence of the flux can be expressed as

$$\nabla\cdot\mathbf{J} = A_1 + A_2 + \nabla\cdot\mathbf{A}_3 + \nabla\cdot\mathbf{A}_4 \tag{3.25}$$

with

$$\begin{aligned}
A_1 &= \left[(-m^{-1}\nabla_{\mathbf{X}}\Phi)\cdot\nabla_{\mathbf{v}}E + (\mathbf{v})\cdot\nabla_{\mathbf{X}}E\right](-k_BT)^{-1}\Psi_{\text{GB}} \\
A_2 &= \left[\nabla_{\mathbf{v}}\cdot(-m^{-1}\nabla_{\mathbf{X}}\Phi) + \nabla_{\mathbf{X}}\cdot(\mathbf{v})\right]\Psi_{\text{GB}} \\
\mathbf{A}_3 &= -\frac{1}{2}(\nabla\cdot\overline{\mathbb{G}})\Psi_{\text{GB}} \\
\mathbf{A}_4 &= \mathbf{A}_4^{(1)} + \mathbf{A}_4^{(2)} \\
\mathbf{A}_4^{(1)} &= \begin{bmatrix} \rho^{-1}\mu\wp\mathcal{L}_f - \rho^{-1}\wp\Lambda\Upsilon\Gamma + \rho^{-1}\wp\Lambda\Upsilon \\ -m^{-1}\Upsilon - m^{-1}\Upsilon\Gamma \\ 0 \end{bmatrix}\Psi_{\text{GB}} \\
\mathbf{A}_4^{(2)} &= (2k_BT)^{-1}\begin{bmatrix} \overline{\mathbb{G}}_{\mathbf{uu}}\nabla_{\mathbf{u}}E + \overline{\mathbb{G}}_{\mathbf{uv}}\nabla_{\mathbf{v}}E + \overline{\mathbb{G}}_{\mathbf{uX}}\nabla_{\mathbf{X}}E \\ \overline{\mathbb{G}}_{\mathbf{vu}}\nabla_{\mathbf{u}}E + \overline{\mathbb{G}}_{\mathbf{vv}}\nabla_{\mathbf{v}}E + \overline{\mathbb{G}}_{\mathbf{vX}}\nabla_{\mathbf{X}}E \\ \overline{\mathbb{G}}_{\mathbf{Xu}}\nabla_{\mathbf{u}}E + \overline{\mathbb{G}}_{\mathbf{Xv}}\nabla_{\mathbf{v}}E + \overline{\mathbb{G}}_{\mathbf{XX}}\nabla_{\mathbf{X}}E \end{bmatrix}\Psi_{\text{GB}}.
\end{aligned} \tag{3.26}$$

The energy of the discretized system we introduced in equation 3.11 has gradients

$$\nabla_{\mathbf{u}_\mathbf{n}}E = \rho\mathbf{u}(\mathbf{x}_\mathbf{n})\Delta x_\mathbf{n}^3 \tag{3.27}$$

$$\nabla_{\mathbf{v}_q}E = m\mathbf{v}_q \tag{3.28}$$

$$\nabla_{\mathbf{X}_q}E = \nabla_{\mathbf{X}_q}\Phi. \tag{3.29}$$

In our notation to simplify the expressions, we have suppressed explicitly denoting the fields on which the operators act with this information easily inferred from equation 3.12.

To show the invariance of Ψ_{GB} under the stochastic dynamics, we show that each of the terms $A_1, A_2, \mathbf{A}_3, \mathbf{A}_4$ is zero. The expression A_1 is closely related to the time derivative of the energy under the non-dissipative dynamics of the microstructures. We find after direct substitution of the energy gradients and cancellations that $A_1 = 0$. The term A_2 has important implications for the transport of probability mass on the phase-space of $(\mathbf{u}, \mathbf{v}, \mathbf{X})$. It can be interpreted as the phase-space compressibility associated with transport by the vector field of the non-dissipative dynamics of the system $(0, -m^{-1}\nabla_{\mathbf{X}}\Phi, \mathbf{v})$. The $A_2 = 0$ is zero since each term depends on distinct degrees of freedom from those appearing in the gradient being taken. This is closely related to the Hamiltonian structure of our non-dissipative dynamics which have conjugate configuration and momentum degrees of freedom [4]. The term A_3 arises from fluxes driven by multiplicative noise in the stochastic driving fields of the system [16]. In the present setting, the multiplicative noise has a rather special form in which only the particle configuration $\mathbf{X}$ plays a role in modulating the noise covariance $\overline{\mathbb{G}}$. This enters through the terms Γ, Λ which appear only in $\overline{\mathbb{G}}_{\mathbf{u},\mathbf{u}}$ and $\overline{\mathbb{G}}_{\mathbf{u},\mathbf{v}}$, see equation 3.19. Since each term depends on distinct degrees of freedom from those appearing in the gradient being taken, we have the term $A_3 = 0$.

This leaves $\mathbf{A}_4$, which accounts for the balance between the dissipation and stochastic fluctuations of the system. An important issue is how the projection operator enforcing incompressibility impacts this fluctuation-dissipation balance. The first covariance term in

$\mathbf{A}_4$ in equation 3.26 can be expanded using properties of our projection operator and discrete energy to obtain

$$\begin{aligned}(\overline{\mathbb{G}}_{\mathbf{uu}}\nabla_{\mathbf{u}}E)(2k_BT)^{-1} &= \rho^{-1}\mu\wp\mathcal{L}_f\wp^T\mathbf{u} - \rho^{-1}\wp\Lambda\Upsilon\Gamma\wp^T\mathbf{u} \\ &= \rho^{-1}\mu\wp\mathcal{L}_f\mathbf{u} - \rho^{-1}\wp\Lambda\Upsilon\Gamma\mathbf{u}.\end{aligned} \tag{3.30}$$

We have used the property that our discrete $\wp$ defined in equation 3.15 is an exact projection operator so that $\wp^T = \wp$. We have also used that the incompressibility constraint is imposed exactly so that the fluid velocity field at any given time satisfies $\mathbf{u} = \wp\mathbf{u}$. By a similar argument, we have

$$(\overline{\mathbb{G}}_{\mathbf{vu}}\nabla_{\mathbf{u}}E)(2k_BT)^{-1} = m^{-1}\wp\Upsilon\Gamma\wp^T\mathbf{u} = m^{-1}\wp\Upsilon\Gamma\mathbf{u} \tag{3.31}$$

$$(\overline{\mathbb{G}}_{\mathbf{uv}}\nabla_{\mathbf{v}}E)(2k_BT)^{-1} = \rho^{-1}\wp\Lambda\Upsilon\wp^T\mathbf{v} = \rho^{-1}\wp\Lambda\Upsilon\mathbf{v}. \tag{3.32}$$

We have used throughout that the projection operator $\wp$ when extended to all of the degrees of freedom of the system does not effect directly the microstructure configuration or velocity so in fact $\mathbf{v} = \wp\mathbf{v}$ and $\mathbf{X} = \wp\mathbf{X}$. The components of $\overline{\mathbb{G}}$ associated with $\mathbf{X}$ are all zero $\overline{\mathbb{G}}_{\mathbf{X},(\cdot)} = \overline{\mathbb{G}}_{(\cdot),\mathbf{X}} = 0$. Using these results in equation 3.26 and canceling common terms yields that $\mathbf{A}_4 = 0$. This shows that $\nabla \cdot \mathbf{J} = 0$.

We have shown that the Gibbs-Boltzmann distribution is invariant under the projected stochastic dynamics given in equations 3.12– 3.14. These results show that it is sufficient to ensure thermal fluctuations consistent with statistical mechanics by using our combined approach of (i) imposing exactly a fluctuation-dissipation condition to obtain a discretization of the stochastic driving fields [5, 4, 1], along with, (ii) imposing the incompressibility constraint with an exact projection $\wp$, [5, 3, 4]. The first condition ensures the discretization properly balances the stochastic driving fields with the dissipative properties of the discrete operators. The second condition using an exact projection ensures that the incompressibility constraint does not introduce new discretization artifacts which adversely effect the propagation of thermal fluctuations through the discretized system. The general principles we have presented here, and in the prior works [4, 5, 1], can be applied broadly to obtain discretizations for incompressible fluctuating hydrodynamics and other spatially extended stochastic systems.

An interesting point to remark is that the no-slip boundary conditions did not require any explicit consideration in our analysis above. However, they were tacitly included through the precise definition of the discrete dissipative operators and the particular form taken by the projection operator $\wp$. The effective action of these operators on the degrees of freedom representing the state of the system in the interior of the domain is influenced by the boundary conditions. For instance, the stencil of the discrete operators change at locations adjacent to the no-slip boundary. An important feature of our discretization approach for the stochastic driving fields, is that our fluctuation-dissipation condition naturally handles the augmented behaviors of the dissipative operators near the boundaries caused by the no-slip conditions. These features highlight the utility of our approach of using statistical mechanics principles to approximate the stochastic driving fields to obtain practical numerical methods for spatially extended stochastic equations [4, 5, 1].

3.3. Efficient Generation of the Stochastic Driving Fields. We have shown that imposing an exact fluctuation-dissipation balance on the semidiscretized stochastic dynamics provides a derivation of effective stochastic driving fields in the discrete setting that yield thermal fluctuations consistent with statistical mechanics. An important challenge in practice is to generate efficiently these discrete stochastic driving fields having the specific spatial covariance $\mathbb{G}$ given in equation 3.19. A natural approach for generating multivariate Gaussians $\boldsymbol{\xi}$ with a specified covariance structure $\langle\boldsymbol{\xi}\boldsymbol{\xi}^T\rangle = G$ is to perform a factorization $G = HH^T$ and use standard Gaussian variates $\boldsymbol{\eta}$ with $\langle\boldsymbol{\eta}\boldsymbol{\eta}^T\rangle = I$ to generate $\boldsymbol{\xi} = H\boldsymbol{\eta}$. This follows since $\langle\boldsymbol{\xi}\boldsymbol{\xi}^T\rangle = \langle H\boldsymbol{\eta}\boldsymbol{\eta}^T H^T\rangle = HH^T = G$. For this to be effective, a key issue is to have a factor H whose action on a vector can be computed efficiently and to determine

efficiently the factor H itself from G. Unfortunately, the most straight-forward method of using Cholesky factorization to obtain H from G has a computational cost of $O(N^3)$ and typically yields a dense factor which would incur a cost of $O(N^2)$ each time we generate the stochastic driving fields. Here N is the total number of mesh degrees of freedom which for problems in three spatial dimensions would be rather large.

We shall take another approach to generate the random variates with $O(N\log(N))$ computational cost by using special properties of the stochastic dynamics and the discrete operators. We first factor G into a form that decouples the microstructure and fluid degrees of freedom. This is accomplished by expressing the stochastic driving fields $\mathbf{f}_{thm}, \mathbf{F}_{thm}$ in terms of $\mathbf{g}_{thm} = \mathbf{f}_{thm} + \Lambda\mathbf{F}_{thm}$ as in [4]. This has the convenient property that the spatial covariances becomes

$$\langle \mathbf{g}_{thm}\mathbf{g}_{thm}^T\rangle = G = -2k_BT\mu\mathcal{L}_f \tag{3.33}$$
$$\langle \mathbf{F}_{thm}\mathbf{F}_{thm}^T\rangle = 2k_BT\Upsilon \tag{3.34}$$
$$\langle \mathbf{g}_{thm}\mathbf{F}_{thm}^T\rangle = 0. \tag{3.35}$$

A particularly important property is that $\mathbf{F}_{thm}$ and $\mathbf{g}_{thm}$ are now decorrelated Gaussian variates that can be generated independently. The original stochastic driving fields can be recovered by using that $\mathbf{f}_{thm} = \mathbf{g}_{thm} - \Lambda\mathbf{F}_{thm}$. In the case that Υ is a scalar as is assumed in our current presentation the variate $\mathbf{F}_{thm}$ can be generated trivially having $O(N)$ computational cost. This reduces the problem to that of generating efficiently the variates $\mathbf{g}_{thm}$.

To generate $\mathbf{g}_{thm}$ we shall use that its covariance structure G given in equation 3.33 can be diagonalized into the form $D = PGP^T$ where D is diagonal and P provides a unitary change of basis. We generate the random field using $\mathbf{g}_{thm} = P^T\sqrt{D}\boldsymbol{\eta}$, where $\boldsymbol{\eta}$ is a complex-valued Gaussian random variate with $\langle\boldsymbol{\eta}\overline{\boldsymbol{\eta}}^T\rangle = I$. This requires we determine the diagonal factor D and the necessary transforms to compute the action of P^T. Since $\boldsymbol{\eta}$ is complex-valued, to fully determine its statistics also requires that we determine the covariance between the real and imaginary components and also impose conditions that ensure a real-valued stochastic field $\mathbf{g}_{thm}$.

For the specific spatial discretization introduced for the channel geometry in Section 3, we have that the discrete Laplacian $\mathcal{L}_f$ subject to the no-slip boundary conditions is diagonalized by the transform $P = S_zF_yF_x$, where S_z denotes for the z-direction the Fast Sine Transform (FST) and F_x,F_y denotes for the xy-direction the standard Fast Fourier Transform (FFT) [11, 28]. The Fourier symbols yielding D for our discrete Laplacian can be computed with computational cost $O(N\log(N))$, which needs to be performed only once for the discretization mesh. We use in our algorithms the complex exponential form of the Fast Fourier Transforms. The generation of the stochastic driving fields is accomplished by computing $\mathbf{g}_{thm} = F_x^TF_y^TS_z^T\sqrt{D}\boldsymbol{\eta}$, where the complex-valued $\boldsymbol{\eta}$ satisfies $\langle\boldsymbol{\eta}\overline{\boldsymbol{\eta}}^T\rangle = I$.

To make this generation procedure work in practice there are some important additional considerations. Since complex values are used in Fourier-space, there are multiple ways to satisfy the condition $\langle\boldsymbol{\eta}\overline{\boldsymbol{\eta}}^T\rangle = I$. In fact, to determine fully the statistics of the Gaussian variate $\boldsymbol{\eta}$ also requires specification of the other covariance components between the various real and imaginary components of $\boldsymbol{\eta}$. A related issue is that the generated stochastic field $\mathbf{g}_{thm}$ must be real-valued. This latter requirement provides additional important conditions on $\boldsymbol{\eta}$. We now discuss in more detail for the discretization our procedure for generating such a complex-valued Gaussian.

Corresponding to the transforms F_x, F_y, S_z we index the Fourier modes using the wave-vector notation $\mathbf{k} = (\ell, m, n)$. We define the *conjugate mode* to $\mathbf{k}$ as the mode with index $\overline{\mathbf{k}} = \sigma\mathbf{k} = (-\ell, -m, n)$. We define the *Hermitian transpose* as $\boldsymbol{\eta}_{\mathbf{k}}^H = \overline{\boldsymbol{\eta}}_{\mathbf{k}}^T$ which we also refer to as the *conjugate transpose*. For the Fourier modes under the inverse transform $P^T = F_x^TF_y^TS_z^T$ to yield a real-valued field requires the *conjugacy condition* $\overline{\boldsymbol{\eta}}_{\mathbf{k}} = \boldsymbol{\eta}_{\sigma\mathbf{k}}$. From these considerations we have for Fourier modes corresponding to a real-valued field that $\boldsymbol{\eta}_{\mathbf{k}}^H = \overline{\boldsymbol{\eta}}_{\mathbf{k}}^T = \boldsymbol{\eta}_{\sigma\mathbf{k}}^T$. The condition $\langle\boldsymbol{\eta}\overline{\boldsymbol{\eta}}^T\rangle = I$ takes on the form for the individual modes

$\langle \boldsymbol{\eta}_{\mathbf{k}} \overline{\boldsymbol{\eta}}_{\mathbf{k}}^T \rangle = I$, where I for the modes denotes the three by three identity matrix. The real-valued conjugacy condition gives that $\overline{\boldsymbol{\eta}}_{\mathbf{k}} = \boldsymbol{\eta}_{\sigma\mathbf{k}}$. By letting $\mathbf{k}'' = \sigma\mathbf{k}'$ we have the two conditions

$$\langle \boldsymbol{\eta}_{\mathbf{k}} \overline{\boldsymbol{\eta}}_{\mathbf{k}'}^T \rangle = I\delta_{\mathbf{k},\mathbf{k}'} \tag{3.36}$$
$$\langle \boldsymbol{\eta}_{\mathbf{k}} \boldsymbol{\eta}_{\mathbf{k}''}^T \rangle = I\delta_{\mathbf{k},\sigma\mathbf{k}''}. \tag{3.37}$$

The $\delta_{\mathbf{m},\mathbf{n}}$ denotes the Kronecker δ-function. We now show for $\boldsymbol{\eta}$ these two conditions fully determine the statistics of the real and imaginary components $\boldsymbol{\eta} = \boldsymbol{\alpha} + i\boldsymbol{\beta}$. The conditions take the form

$$\langle \boldsymbol{\eta}_{\mathbf{k}} \overline{\boldsymbol{\eta}}_{\mathbf{k}'}^T \rangle = \left(\langle \boldsymbol{\alpha}_{\mathbf{k}} \boldsymbol{\alpha}_{\mathbf{k}'}^T \rangle + \langle \boldsymbol{\beta}_{\mathbf{k}} \boldsymbol{\beta}_{\mathbf{k}'}^T \rangle \right) + i \left(\langle \boldsymbol{\beta}_{\mathbf{k}} \boldsymbol{\alpha}_{\mathbf{k}'}^T \rangle - \langle \boldsymbol{\alpha}_{\mathbf{k}} \boldsymbol{\beta}_{\mathbf{k}'}^T \rangle \right) = I\delta_{\mathbf{k},\mathbf{k}'} \tag{3.38}$$
$$\langle \boldsymbol{\eta}_{\mathbf{k}} \boldsymbol{\eta}_{\mathbf{k}''}^T \rangle = \left(\langle \boldsymbol{\alpha}_{\mathbf{k}} \boldsymbol{\alpha}_{\mathbf{k}''}^T \rangle - \langle \boldsymbol{\beta}_{\mathbf{k}} \boldsymbol{\beta}_{\mathbf{k}''}^T \rangle \right) + i \left(\langle \boldsymbol{\alpha}_{\mathbf{k}} \boldsymbol{\beta}_{\mathbf{k}''}^T \rangle + \langle \boldsymbol{\beta}_{\mathbf{k}} \boldsymbol{\alpha}_{\mathbf{k}''}^T \rangle \right) = I\delta_{\mathbf{k},\sigma\mathbf{k}''}. \tag{3.39}$$

By equating the real and imaginary parts in each expression gives the conditions

$$\langle \boldsymbol{\alpha}_{\mathbf{k}} \boldsymbol{\alpha}_{\mathbf{k}'}^T \rangle + \langle \boldsymbol{\beta}_{\mathbf{k}} \boldsymbol{\beta}_{\mathbf{k}'}^T \rangle = I\delta_{\mathbf{k},\mathbf{k}'} \tag{3.40}$$
$$\langle \boldsymbol{\alpha}_{\mathbf{k}} \boldsymbol{\alpha}_{\mathbf{k}''}^T \rangle - \langle \boldsymbol{\beta}_{\mathbf{k}} \boldsymbol{\beta}_{\mathbf{k}''}^T \rangle = I\delta_{\mathbf{k},\sigma\mathbf{k}''} \tag{3.41}$$
$$\langle \boldsymbol{\beta}_{\mathbf{k}} \boldsymbol{\alpha}_{\mathbf{k}'}^T \rangle - \langle \boldsymbol{\alpha}_{\mathbf{k}} \boldsymbol{\beta}_{\mathbf{k}'}^T \rangle = 0 \tag{3.42}$$
$$\langle \boldsymbol{\alpha}_{\mathbf{k}} \boldsymbol{\beta}_{\mathbf{k}''}^T \rangle + \langle \boldsymbol{\beta}_{\mathbf{k}} \boldsymbol{\alpha}_{\mathbf{k}''}^T \rangle = 0. \tag{3.43}$$

By linearly combining the equations this yields the conditions

$$\langle \boldsymbol{\alpha}_{\mathbf{k}} \boldsymbol{\alpha}_{\mathbf{k}'}^T \rangle = \frac{1}{2} I \left(\delta_{\mathbf{k},\mathbf{k}'} + \delta_{\mathbf{k},\sigma\mathbf{k}'} \right) \tag{3.44}$$
$$\langle \boldsymbol{\beta}_{\mathbf{k}} \boldsymbol{\beta}_{\mathbf{k}'}^T \rangle = \frac{1}{2} I \left(\delta_{\mathbf{k},\mathbf{k}'} - \delta_{\mathbf{k},\sigma\mathbf{k}'} \right) \tag{3.45}$$
$$\langle \boldsymbol{\alpha}_{\mathbf{k}} \boldsymbol{\beta}_{\mathbf{k}'}^T \rangle = 0. \tag{3.46}$$

The last condition shows that real and imaginary components of the modes of the Gaussian $\boldsymbol{\eta}$ should be generated to be statistically independent. The condition that the generated stochastic field be real-valued has the important consequence that the random Gaussian variate for the real part $\boldsymbol{\alpha}_{\mathbf{k}}$ must always be exactly the same as the value $\boldsymbol{\alpha}_{\sigma\mathbf{k}}$ and the random Gaussian variate for the imaginary part $\boldsymbol{\beta}_{\mathbf{k}}$ must always be exactly the negative of the value $\boldsymbol{\beta}_{\sigma\mathbf{k}}$. In the special case of self-conjugate modes $\mathbf{k} = \sigma\mathbf{k}$, the conditions require that the imaginary part is zero $\boldsymbol{\beta}_{\mathbf{k}} = 0$ and the contributions to the random field are only made by the real part $\langle \boldsymbol{\alpha}_{\mathbf{k}} \boldsymbol{\alpha}_{\mathbf{k}}^T \rangle = I$. This provides the details of how to generate the modes $\boldsymbol{\eta}_{\mathbf{k}}$ in Fourier space to obtain the required complex-valued Gaussian random variates $\boldsymbol{\eta}$. This can be accomplished in Fourier space with a computational cost of $O(N)$. By performing the inverse transforms this provides an efficient method with computational cost $O(N \log(N))$ to generate the stochastic driving field $\mathbf{g}_{thm}$. We remark that the effects of the no-slip boundary conditions were tacitly taken into account in our stochastic field generation through the specific form taken by the Fourier symbols in the diagonal operator D and the form of the inverse transforms used.

4. Validation Studies.

4.1. Covariance obtained from the Stochastic Field Generator. To validate our methods for generating the stochastic driving field $\mathbf{g}_{thm}$ in Section 3.3, we consider the discretization of the channel domain with $20 \times 20 \times 20$ cells in each direction introduced in Section 3. We estimate empirically from generated samples of the stochastic driving fields the spatial covariance structure in real-space $\tilde{G}_{\mathbf{m},\mathbf{m}_0} = \langle \mathbf{g}_{\mathbf{m}_0} \mathbf{g}_{\mathbf{m}}^T \rangle$. This is predicted to have the entries of the covariance matrix $G_{\mathbf{m},\mathbf{m}_0} = [2k_B T \mathcal{L}_f]_{\mathbf{m},\mathbf{m}_0}$. These entries correspond proportionally to our face-centered approximation of the Laplacian by central differences. The correlation structure is sparse and involves a positive entry when $\mathbf{m} = \mathbf{m}_0$ and a negative

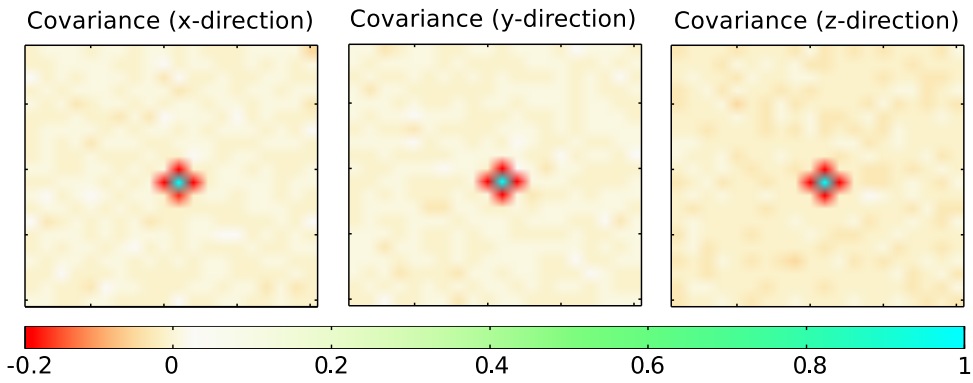

FIG. 4.1. *Spatial Covariance Structure of* $\mathbf{g}_{thm}$. *We consider the covariance of the stochastic fields generation by the method introduced in Section 3.3 for the staggered mesh discretization of the channel geometry with* $20 \times 20 \times 20$ *mesh cells in each direction. We empirically estimate the covariance using* $\langle \mathbf{g}_{\mathbf{m}_0} \mathbf{g}_{\mathbf{m}}^T \rangle$ *where* $\mathbf{m}_0$ *denotes the index of a grid cell near the center of the channel. The estimated covariance structure in each direction agrees well with the prediction based on the face-centered discrete Laplacian operator* $\mathcal{L}_f$ *and equation 3.33.*

entry for each $\mathbf{m}$ corresponding to the nearest neighbors in each of the Cartesian directions. We show the spatial correlation estimated empirically for a cross-section of the mesh for each of the velocity components in Figure 4.1. We find good agreement between the predicted covariance structure and those obtained from our stochastic field generation method introduced in Section 3.3.

4.2. Brownian Motion of a Particle Diffusing in a Harmonic Potential. We validate our computational methods for the microstructure dynamics coupled using fluctuating hydrodynamics by considering the Brownian motion of a particle diffusing in the harmonic potential $\Phi(\mathbf{X}) = \frac{1}{2} K \mathbf{X}^2$. We use for the spring stiffness $K = k_B T$, particle mass $m = 19200$ amu, and temperature $T = 298.15$ Kelvin ($k_B T = 2.479$ nm$^2 \cdot$ amu $\cdot$ ps^{-2}). The computational domain is taken to be 30nm $\times$ 30nm $\times$ 30nm resolved with a grid having cells with mesh-width 1 nm. For this choice of parameters, the Gibbs-Boltzmann distribution $\rho(\mathbf{X}) = (1/Z) \exp(-\Phi(\mathbf{X})/k_B T)$ predicts a standard deviation in position of $\sqrt{k_B T/K} = 1$ nm. The Maxwellian for the velocity fluctuations predicts a standard deviation $\sqrt{k_B T/m} = 11.36$ nm/ns [29]. We performed simulations with $\Delta t = 0.15$ns for $50,000$ time-steps and estimated the position and velocity distributions. We find that our stochastic numerical methods yield an appropriate effective temperature for the microstructure and that the fluctuations in configuration agree well with the Gibbs-Boltzmann distribution, see Figure 4.2.

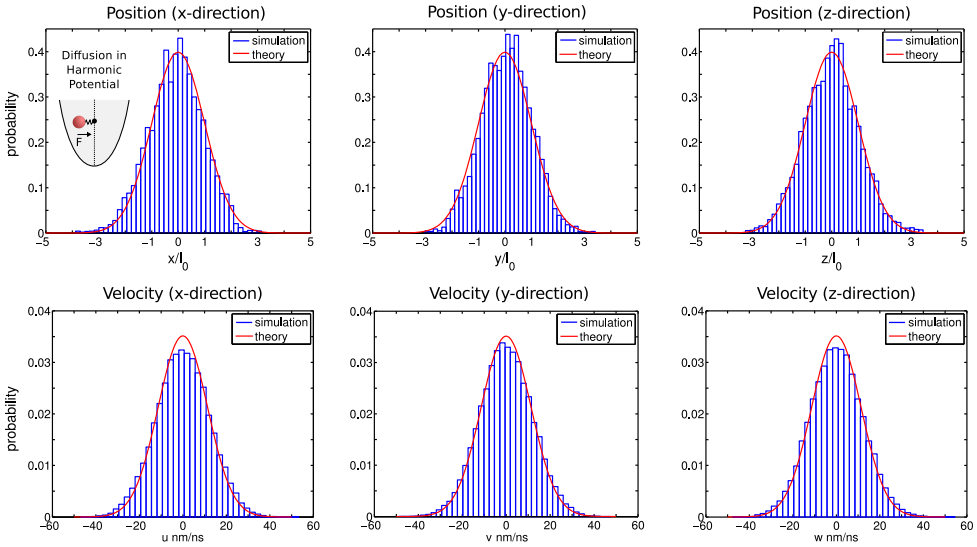

FIG. 4.2. *Brownian Motion of a Particle Diffusing in a Harmonic Potential. The probability distribution for the particle location and velocity are estimated from a single trajectory simulated with our stochastic numerical methods. The velocity distribution is found to be in good agreement with the predicted Maxwellian. The position distribution is found to be in good agreement with the Gibbs-Boltzmann distribution.*

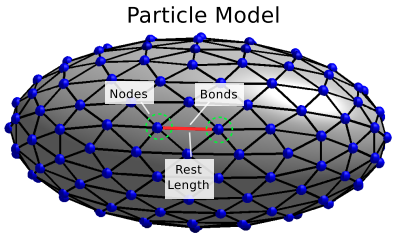

FIG. 4.3. *Particle Model. We model the geometry and hydrodynamic responses of spherical and ellipsoidal colloids by using a collection of control nodes distributed on the particle surface that are coupled through harmonic springs with a specified rest-length. The control node distribution is obtained by starting with a scaled icosahedron and bisecting the edges recursively. The restoring forces of the harmonic bonds act to enforce an approximate rigid-body no-slip response to the surrounding fluid.*

5. Simulations of Ellipsoidal Colloids and Confinement Effects. To simulate the diffusion and hydrodynamic responses of ellipsoidal colloids subject to confinement effects within a channel, we develop a model based on control nodes connected by harmonic bonds with a specified rest-length as shown in Figure 4.3. The control node distribution is obtained by starting with a scaled icosahedron and bisecting the edges recursively. Similar types of models have been developed in [23, 2, 19]. We choose the strength of the bonds sufficiently strong that a rigid-body no-slip response is obtained for the hydrodynamics. We consider how this model behaves in practice as a model for ellipsoids of different aspect ratios by making comparisons with the classical analytic results of Perrin [13, 26].

5.1. Translational and Rotational Mobility. We consider prolate ellipsoidal colloids with semi-major axis a and semi-minor axes $b = c$. For such colloidal particles in a bulk Newtonian fluid, the translational mobility has been analytically predicted by Perrin as [13, 26]

$$M_{\text{trans}} = \frac{\ln\left(p^{-1}[1+(1-p^2)^{1/2}]\right)}{6\pi\mu a(1-p^2)^{1/2}}, \quad \text{where} \quad p = \frac{c}{a}. \tag{5.1}$$

In this expression we take into account the correction to the typo that was found in the original paper by Perrin in the statement of equation (41) [26, 13]. For the rotational mobility of prolate ellipsoids in response to an applied torque Chwang and Wu[10] analytically predict

$$M_{\text{rot}} = \frac{1}{8\pi\mu a b^2 C_M}, \quad C_M = \frac{4q^3}{3(2q-(1-q^2)\ln\left(\frac{1+q}{1-q}\right))} \tag{5.2}$$

where $q = \sqrt{1-(b/a)^2}$.

We compare the hydrodynamic responses of our colloidal model to these results. To use our computational methods but to minimize the effects of the wall in these studies, we consider computational domains where the channel has a width of about 10 times the particle radius. To probe the translational mobility of our model, we applied a unit force over the surface of our particle and measured from our simulations the resulting steady-state velocity of the ellipsoidal particle. To probe the rotational mobility of our model, we applied a unit torque as an averaged force distribution over the surface of our particle and measured the angular velocities by averaging moments over the particle surface. We found that the translational and rotational hydrodynamic responses of our particle model agree quite well with the analytic when using an effective radius for our particle of $a = 5.45$, see Figure 5.1. The translational mobilities showed very good agreement for all of the aspect ratios considered. The primary discrepancies occurred for the rotational mobilities as the aspect ratio became small.

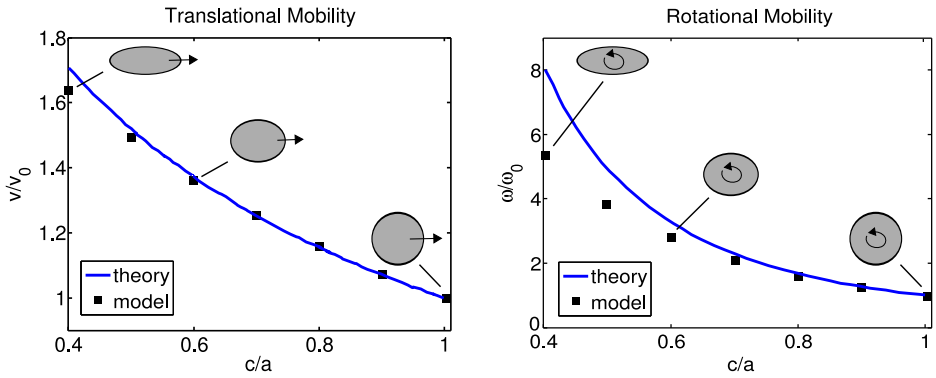

FIG. 5.1. *Comparison of the Translational and Rotational Mobilities of our Colloid Model with Theory. We find that our colloidal model yields hydrodynamic responses in good agreement with the analytic predictions for the translational and rotational mobilities of ellipsoidal particles given in equation 5.1 and equation 5.2. The primary discrepancy occurs for the rotational mobilities when the ellipsoidal particles have small aspect ratio.*

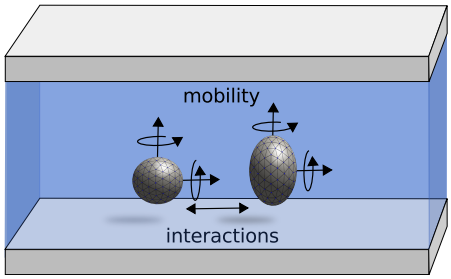

FIG. 5.2. *Confinement of Spherical and Ellipsoidal Particles in a Channel and Effects on Hydrodynamic Responses. Confinement is expected to effect significantly the mobility and hydrodynamic interactions between particles when confined with a channel. The hydrodynamic responses and coupling is expected to change depending on the distance of particles to the channel walls.*

5.2. Effects of Confinement on the Mobility and Hydrodynamic Interactions of Particles. We explore the role that confinement effects play on mobility and hydrodynamic interactions between the particles. We investigate responses for (i) a spherical particle having radius $r = 5$ nm and an ellipsoidal particle having $a = 5$ nm, $b = c = 2.5$ nm. We consider a channel with walls separated by 30nm in the z-direction and a span of 120nm in the periodic xy-directions. We resolve this channel geometry using a discretization having mesh-width 1nm in each direction.

We investigate how the translational and rotational mobilities change as the colloidal particle occupies distances to one of the walls ranging from 10nm to 2nm. We consider for the ellipsoidal particle the two cases when (i) the semi-major axis is parallel to the channel wall and (ii) the semi-major axis is perpendicular to the channel wall. As a consequence of the symmetry of the channel system under rotation around the z-axis, we only need to consider the responses in the x and z directions.

We find that the translational mobility is impacted significantly by the particles proximity to a channel wall, see Figure 5.3. In contrast, the rotational mobility is only effected significantly by the channel wall when the particle is in close proximity to the wall. These changes in the active responses to force and torque captured by the mobility M have important implications also for the rotational and translational diffusivities D of particles within the channel through the Stokes-Einstein relation $D = 2k_BTM$, [29]. These results indicate that the stochastic methods will also capture how the diffusivity of a particle is augmented by its proximity to the wall.

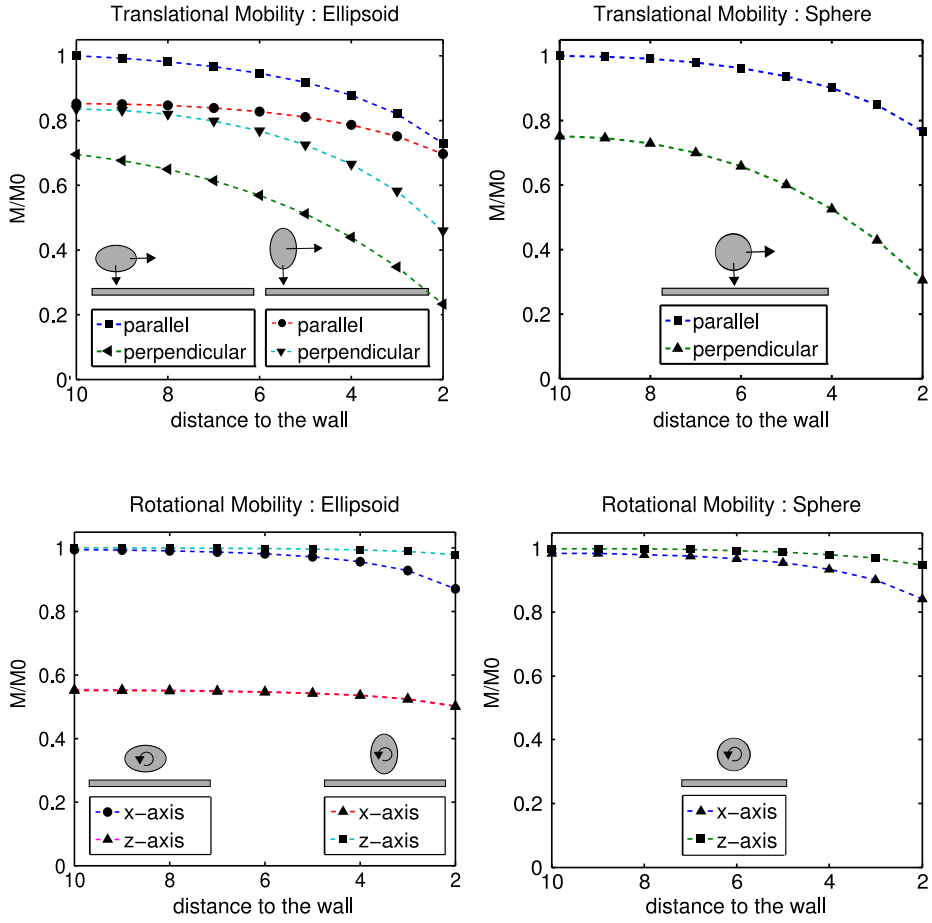

FIG. 5.3. *Effect of Confinement on the Translational and Rotational Mobilities of Spherical and Ellipsoidal Particles. We use our colloid model and computational methods to study the hydrodynamic responses of particles as they approach one of the channel walls. We consider the translational and rotational mobilities obtained from the active responses of particles to an applied force or torque. We find that the translational mobility is impacted most significantly by the particles proximity to a channel wall. In contrast the rotational mobility is only effected by the channel wall when the particle is rather close. The active responses as characterized by the mobility M have important implications also for the passive rotational and translational diffusivities D of particles within the channel through the Stokes-Einstein relation* $D = 2k_BTM$, *[29]. These results indicate that the stochastic methods will also capture how the diffusivity of a particle is augmented by its proximity to the wall.*

5.3. Reduced Model of Ellipsoidal Particles as Trimers. In our studies we expect that many of the hydrodynamic responses of the colloidal particles can be captured to a good approximation by a less detailed geometric description by using only a few control nodes, [23, 2, 19]. To improve the computational efficiency in simulations we use a reduced description that replaces the full geometric approach introduced in Section 5 by instead a trimer of three control nodes linked by harmonic springs of non-zero rest-length. While this reflects the approximate responses of an ellipsoid for one particular aspect ratio, this can also be augmented by adding control nodes arranged either linearly or in a cluster to obtain the approximate responses for other aspect ratios. When comparing the responses of our trimer model with three control nodes that span about 2 mesh-widths of the discretization mesh with the results of Perrin's equation 5.1, we find the trimer approximates a prolate ellipsoid having aspect ratio of $c/a = 0.6$. We use this choice in our subsequent studies.

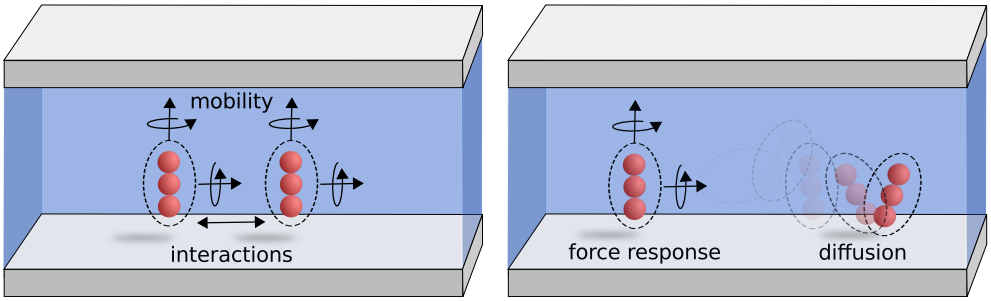

FIG. 5.4. *Confinement Effects on Pair Mobility and Diffusivity for our Reduced Model of Ellipsoidal Particles as Trimers. We use a reduced model to approximate the ellipsoidal particles as a trimer of particles. We find from our mobility results that when the three trimer control nodes span* 2 *mesh-widths this approximates the response of an ellipsoidal particle with aspects ratio* 0.6. *We probe the effects of confinement both on the active pair interactions mediated by hydrodynamics between the ellipsoidal particles and on the passive diffusive responses through correlations in the Brownian motions.*

5.4. Hydrodynamic Interactions and Pair Diffusivity : Translational and Rotational Pair Mobility. We probe the effects of confinement on both the active responses mediated by hydrodynamics between a pair of particles and the passive diffusive correlations in the joint Brownian motions of a pair of particles. We investigate the pair mobility M by studying for a force applied to one particle the hydrodynamic response of the other particle. By the Stokes-Einstein relations the pair diffusivity of particle D is predicted to be

$$D = 2k_B T M. \tag{5.3}$$

The grand-mobility tensor comprising both the translational and rotational responses for the collective particle degrees of freedom $\mathbf{X} = (X_1, X_2)$ can be expressed as

$$\frac{d}{dt}\begin{bmatrix} X_1 \\ X_2 \end{bmatrix} = \begin{bmatrix} M_{11} & M_{12} \\ M_{12} & M_{22} \end{bmatrix} \begin{bmatrix} F_1 \\ F_2 \end{bmatrix}. \tag{5.4}$$

In the current setting we are most interested in the diagonal entries of the M_{11} and M_{12} components which characterize how a force acting on one particle effects the motion of the other in the same direction. We determine these responses empirically by applying such a force and measuring the resulting velocity in our computational simulations.

To estimate empirically the pair diffusivity D of our particles we use

$$D = \frac{1}{\delta t}\langle \Delta\mathbf{X}\Delta\mathbf{X}^T \rangle \tag{5.5}$$

where $\Delta\mathbf{X} = \mathbf{X}(\delta t) - \mathbf{X}(0)$. The components in which we are most interested are the diagonal terms of D_{11} and D_{12} which correspond to how the diffusive motion of one of the particles is correlated with the other in the same direction.

To investigate the role of confinement in particle interactions, we consider both the active force responses and the passive diffusivities and how they depend on both the proximity of the particles to one of the channel walls and the distance of separation between the particles. For the wall proximity, we consider the two specific cases when the particle is located at position $z = 2$nm and $z = 10$nm.

We find that confinement plays a significant role both in the active hydrodynamic interactions between particles and in the passive diffusivity of their correlated Brownian motions. We find that our stochastic numerical methods yield results in close agreement with the Stokes-Einstein relations given in equation 5.3, see Figure 5.5. We think the slight discrepancy in our results comes from the inherent errors in our different estimators to obtain the mobility and diffusivity of a particle from the computational simulations.

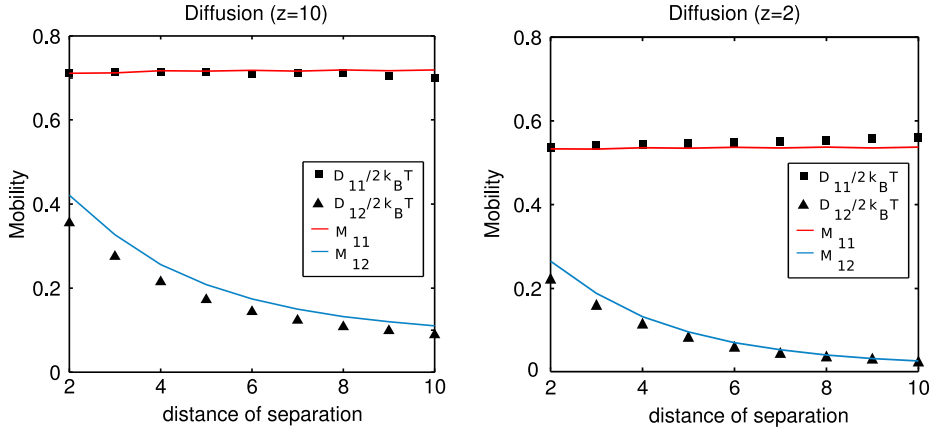

FIG. 5.5. *Confinement Effects on the Pair Mobility and Diffusivity of Particles. We consider the role of proximity to the channel wall both on the active hydrodynamic responses in the interactions between a pair of ellipsoidal particles and on the passive diffusivities in the correlated Brownian motions of the two particles. We find confinement significantly impacts both the active responses and passive diffusivity. We also find that our stochastic computational methods agree to a good approximation with the predictions of the Stokes-Einstein relations $D = 2k_BTM$, [29].*

5.5. Particle Collective Dynamics : Relaxation of Density Fluctuations.

We investigate the collective dynamics of ellipsoidal particles captured by our stochastic numerical methods by considering for a dilute and dense suspension the relaxations observed in the spontaneous density fluctuations. To help enforce sterics between the particles, we introduce a Weeks-Chandler-Andersen interaction between the particles [35]. We study these effects in a channel having a geometry of 60nm × 30nm × 20nm resolved with mesh-width 1nm.

We perform simulations to investigate the collective stochastic dynamics of the hydrodynamically coupled particles in the different density regimes. We perform simulations of (i) a dilute suspension of 100 particles and (ii) and dense suspension of 840 particles, see Figure 5.6. To investigate the role of the hydrodynamic coupling, we perform simulations (i) with our SELM stochastic numerical methods and (ii) with standard Langevin dynamics without hydrodynamic coupling.

To characterize how the density effects the motions of particles we consider for the SELM simulations the translational Mean-Squared Displacement (MSD) and the rotational

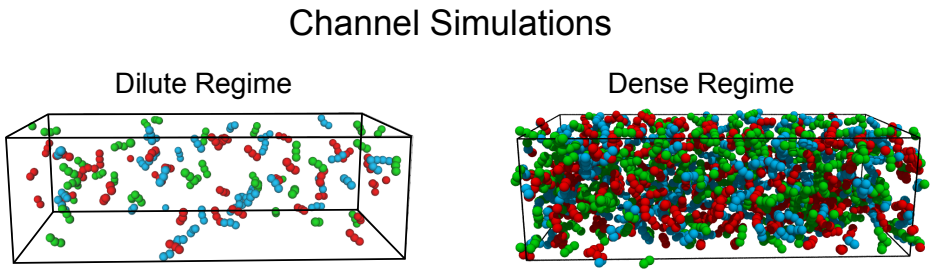

FIG. 5.6. *Ellipsoidal Particles in a Channel. We simulate both a dilute regime consisting of* 100 *particles interacting within a channel and a dense regime with* 840 *particles interacting within a channel. The ellipsoidal particles are represented using our trimer model. Shown are typical configurations of the particles in each of these regimes.*

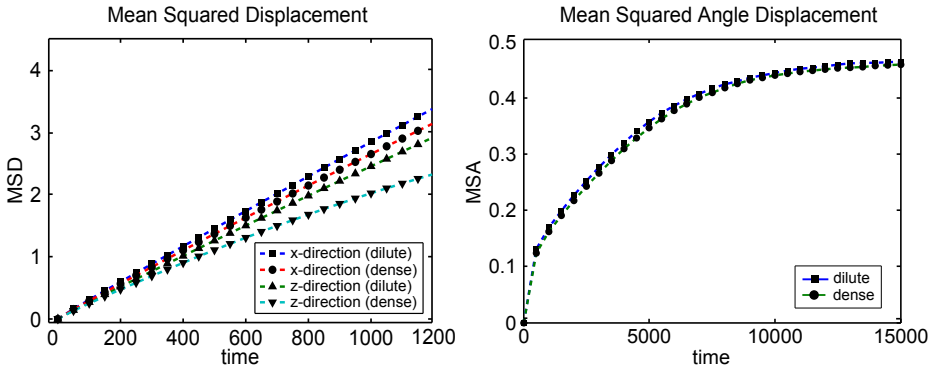

FIG. 5.7. *Mean-Squared Displacement. We consider the translational mean-squared displacement (MSD) and the rotational mean-squared angular displacements (MSA). We find the translational MSD is most effected by the increase in particle density and exhibits a noticeable decrease for the more dense regime. We find the MSA is rather insensitive to the density of particles.*

Mean-Squared Angular Displacement (MSA), see Figure 5.7. We find a noticeable decrease in the MSD as the density increases. This indicates that in the dense case the particle interactions significantly restrict the diffusive motions of the particles. We find that the rotational diffusivity of particles was largely unaffected. This lack of sensitivity is somewhat expected given the more local nature of angular diffusion which only requires rotation locally at a relatively fixed location requiring less collective rearrangements of the particles.

To give a sense of how particles arrange within the channel we show the position distribution and angular distribution in Figure 5.8. We find that the particles distribute almost uniformly throughout the channel but do have a small depletion layer near the channel wall on a length-scale comparable to the radius of the particles. We also find that the angular distribution for pairs of particles exhibits a sinusoidal shape $\rho(\theta) = \frac{\pi}{2}\sin(\theta)$ that is consistent with an isotropic orientation of the ellipsoidal particles within the channel. This distribution follows from the three dimensional geometry associated with the angle between a pair of particles. If one places the director of one particle at the north-pole of the sphere and chooses the other uniformly over the sphere the distribution $\rho(\theta)$ is easily obtained by integrating the spherical coordinates for three dimensional systems. These results indicate there is no

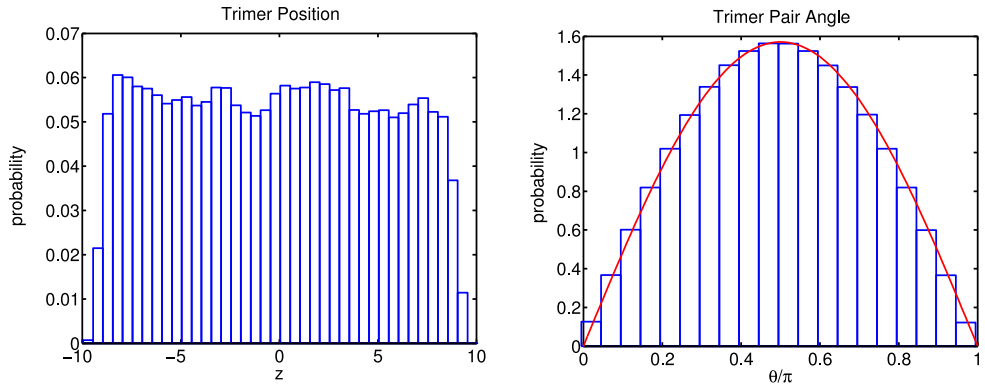

FIG. 5.8. *Distribution of Particles within the Channel. We find the particles distribute uniformly across the channel diameter with the density decreasing in a layer near the boundary on a length-scale comparable to the particle size. We find the angular distribution for pairs of ellipsoidal particles is well-approximated by* $\rho(\theta) = \frac{\pi}{2}\sin(\theta)$. *This is consistent with isotropic arrangements of the particles corresponding to the angle distribution of directors uniformly distributed on the surface of a sphere.*

noticeable biasing of the distribution in our simulations as a consequence of the symmetry broken by the presence of the channel walls.

To investigate the density relaxations of the system, we consider for the SELM stochastic numerical methods and standard Langevin dynamics the Intermediate Scattering Functions (ISFs) of the particles. The ISF for a given wave-vector $\mathbf{k}$ is defined by

$$F(\mathbf{k}, t) = \frac{1}{N}\langle \rho(\mathbf{k}, t)\rho(-\mathbf{k}, 0)\rangle \tag{5.6}$$

where the particle density is represented in terms of Fourier modes as

$$\rho(\mathbf{k}, t) = \sum_{j=1}^{N} e^{-i\mathbf{k}\cdot\mathbf{r}_j(t)}. \tag{5.7}$$

For the SELM and Langevin simulations, we find that each ISF are well-approximated by the decay of a single exponential $\exp(-t\Gamma(\mathbf{k}))$. To characterize the rate on which the density fluctuations relax we consider $\Gamma(\mathbf{k})$ over a range of wave-vectors.

We find for the SELM approach the dispersion relation $\Gamma(\mathbf{k})$ have a quadratic trend $\mathbf{k}^2$. In contrast, for the Langevin simulations that neglect hydrodynamic effects, we find that the dispersion relations have a linear trend $\mathbf{k}$. These results show that our stochastic computational methods capture significant collective effects mediated by hydrodynamics that are not found in simulations performed with conventional Langevin dynamics. The role of the density of the particles is also found to play some role in modulating these rates. We find that the rate at which density fluctuations relax for the dense system is noticeably slower than for the dilute system. This is consistent with the additional steric and hydrodynamic interactions which couple the motions of particles more strongly in the dense system. These preliminary results show the ability of our stochastic computational methods to capture for a large number of interacting particles both the roles played by hydrodynamic coupling and thermal fluctuations in the collective dynamics. We plan to pursue more detailed studies in future work.

6. Conclusions. We have developed stochastic computational methods to take into account confinement effects within channel geometries. Our approach is based on fluctuating hydrodynamics and the Stochastic Eulerian Lagrangian Method (SELM) for incorporating

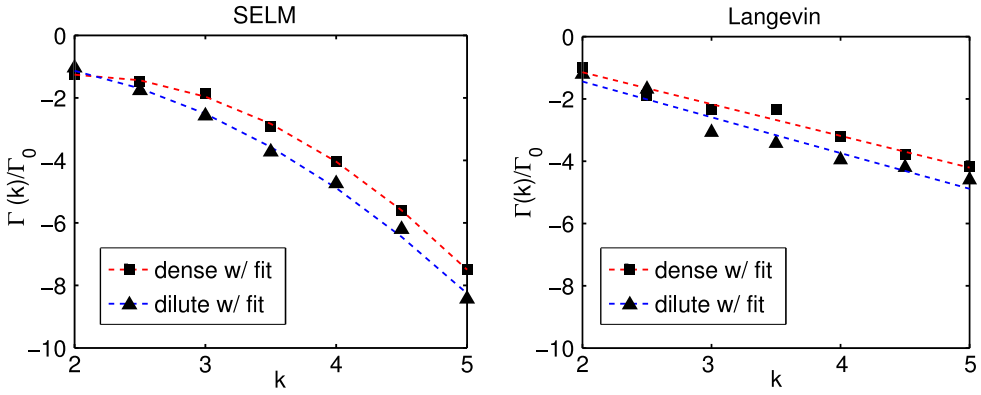

FIG. 5.9. *Relaxation of the Density Fluctuations. The decay of the Intermediate Scattering Functions (ISFs) are fit well by a single exponential* $\exp(-t\Gamma(\mathbf{k}))$ *for both the SELM and Langevin simulations. The dispersion relation* $\Gamma(\mathbf{k})$ *exhibits a quadratic trend* $\mathbf{k}^2$ *for the SELM dynamics incorporating hydrodynamic coupling. The dispersion relation* $\Gamma(\mathbf{k})$ *exhibits a linear trend* $\mathbf{k}$ *for the Langevin dynamics that neglect hydrodynamic effects. The relations are normalized for SELM by* $\Gamma_0 = 0.25$ *and for Langevin by* $\Gamma_0 = 0.005$.

thermal fluctuations into approximate descriptions of the fluid-structure interactions. We have shown our approach of imposing an exact fluctuation-dissipation condition to obtain a discretization of the stochastic driving fields combined with our using an exact projection method to enforce incompressibility is sufficient to ensure results consistent with statistical mechanics. We have shown our stochastic discretization approach also handles naturally fluctuations in the context of the no-slip boundary conditions. We found that the stochastic computational methods work well to capture both on the active hydrodynamic responses and the passive diffusive responses when particles are effected by their proximity to the channel walls. We expect our introduced stochastic computational methods to be applicable broadly to applications in which confinement effects play an important role in the dynamics of microstructures subject to hydrodynamic coupling and thermal fluctuations.

7. Acknowledgements. The authors P.J.A. and Y.W. acknowledge support from the W. M. Keck Foundation. The author P.J.A. acknowledges support from the research grants NSF CAREER DMS-0956210 and DOE CM4. We also acknowledge support from the Center for Scientific Computing at the CNSI and MRL: an NSF MRSEC (DMR-1121053) and NSF CNS-0960316.

REFERENCES

[1] P.J. ATZBERGER, *Spatially adaptive stochastic numerical methods for intrinsic fluctuations in reaction-diffusion systems*, Journal of Computational Physics, 229 (2010), pp. 3474–3501.

[2] P.J. ATZBERGER, *Incorporating shear into stochastic eulerian lagrangian methods for rheological studies of complex fluids and soft materials.*, Physica D-Nonlinear Phenomena, (to appear) (2013).

[3] P. ATZBERGER AND G. TABAK, *Systematic stochastic reduction of inertial fluid-structure interactions subject to thermal fluctuations*, (submitted), (2013).

[4] P. J. ATZBERGER, *Stochastic eulerian lagrangian methods for fluidstructure interactions with thermal fluctuations*, Journal of Computational Physics, 230 (2011), pp. 2821–2837.

[5] P. J. ATZBERGER, P. R. KRAMER, AND C. S. PESKIN, *A stochastic immersed boundary method for fluid-structure dynamics at microscopic length scales*, Journal of Computational Physics, 224 (2007), pp. 1255–1292.

[6] F. BalboaUsabiaga, J. Bell, R. Delgado-Buscalioni, A. Donev, T. Fai, B. Griffith, and C. Peskin, *Staggered schemes for fluctuating hydrodynamics*, Multiscale Model. Simul., 10 (2012), pp. 1369–1408.

[7] Garcia A. L. Williams S. A. Bell, J. B, *Computational fluctuating fluid dynamics*, ESAIM: Mathematical Modelling and Numerical Analysis., 44 (2010), pp. 1085–1105.

[8] Y.-L. Chen, M. D. Graham, J. J. de Pablo, G. C. Randall, M. Gupta, and P. S. Doyle, *Conformation and dynamics of single dna molecules in parallel-plate slit microchannels*, Phys. Rev. E, 70 (2004), pp. 060901–.

[9] A. J. Chorin, *Numerical solution of navier-stokes equations*, Mathematics of Computation, 22 (1968), pp. 745–762.

[10] Allen T. Chwang and T. Yao-Tsu Wu, *Hydromechanics of low-reynolds-number flow. part 1. rotation of axisymmetric prolate bodies*, Journal of Fluid Mechanics, 63 (1974), pp. 607–622.

[11] James W. Cooley and John W. Tukey, *An algorithm for the machine calculation of complex fourier series*, Mathematics of Computation, 19 (Apr., 1965), pp. 297–301.

[12] G. De Fabritiis, M. Serrano, R. Delgado-Buscalioni, and P. V. Coveney, *Fluctuating hydrodynamic modeling of fluids at the nanoscale*, Phys. Rev. E, 75 (2007), pp. 026307–.

[13] Jose Garcia De La Torre and Victor a. Bloomfield, *Hydrodynamic properties of macromolecular complexes. i. translation*, Biopolymers, 16 (1977), pp. 1747–1763.

[14] Knut Drescher, Jrn Dunkel, Luis H. Cisneros, Sujoy Ganguly, and Raymond E. Goldstein, *Fluid dynamics and noise in bacterial cellcell and cellsurface scattering*, Proceedings of the National Academy of Sciences, (2011).

[15] B. Duenweg and A. J. C. Ladd, *Lattice boltzmann simulations of soft matter systems*, arXiv, (2008).

[16] C. W. Gardiner, *Handbook of stochastic methods*, Series in Synergetics, Springer, 1985.

[17] C. K. Choi T. Takagi K. D. Kihm, A. Banerjee, *Near-wall hindered brownian diffusion of nanoparticles examined by three-dimensional ratiometric total internal reflection fluorescence microscopy (3-d r-tirfm)*, Experiments in Fluids, 37 (2004), pp. 811–824.

[18] Mustafa Sabri Kilic and Martin Z. Bazant, *Induced-charge electrophoresis near a wall*, ELECTROPHORESIS, 32 (2011), pp. 614–628.

[19] Yongsam Kim and Ming-Chih Lai, *Simulating the dynamics of inextensible vesicles by the penalty immersed boundary method*, Journal of Computational Physics, 229 (2010), pp. 4840–4853.

[20] Kloeden.P.E. and E. Platen, *Numerical solution of stochastic differential equations*, Springer-Verlag, 1992.

[21] E.M. Lifshitz L.D. Landau, *Course of theoretical physics, Statistical Physics*, Vol. 9, Pergamon Press Oxford, 1980 (Chapter IX).

[22] Po-Keng Lin, Chi-Cheng Fu, Y.-L. Chen, Yan-Ru Chen, Pei-Kuen Wei, C. H. Kuan, and W. S. Fann, *Static conformation and dynamics of single dna molecules confined in nanoslits*, Phys. Rev. E, 76 (2007), pp. 011806–.

[23] D. Liu, E.E. Keaveny, M.R. Maxey, and G.E. Karniadakis, *Force coupling method for flow with ellipsoidal particles*, Journal of Computational Physics, 228 (2009), pp. 3559–3581.

[24] Sumita Pennathur Mariateresa Napoli, Paul Atzberger, *Experimental study of the separation behavior of nanoparticles in micro- and nanochannels*, Microfluidics and Nanofluidics, 10 (2011), pp. 69–80.

[25] B. Oksendal, *Stochastic Differential Equations: An Introduction*, Springer, 2000.

[26] Francis Perrin, *Mouvement brownien d'un ellipsoide (ii) rotation libre et dépolarisation des fluorescences. translation et diffusion de molécules ellipsoidales*, J. Phys. Rad., 7 (1936), pp. 1–11.

[27] Charles S. Peskin, *The immersed boundary method*, Acta Numerica, 11 (2002), pp. 1–39.

[28] W. H. Press, S. A. Teukolsky, W. T. Vetterling, and B. P. Flannery, *Numerical Recipes in C*, Cambridge University Press, Cambridge, 1994.

[29] L. E. Reichl, *A Modern Course in Statistical Physics*, John Wiley and Sons, 1998.

[30] Jon K. Sigurdsson, Frank L.H. Brown, and Paul J. Atzberger, *Hybrid continuum-particle method for fluctuating lipid bilayer membranes with diffusing protein inclusions*, Journal of Computational Physics, 252 (2013), pp. 65–85.

[31] Todd M. Squires and Stephen R. Quake, *Microfluidics: Fluid physics at the nanoliter scale*, Rev. Mod. Phys., 77 (2005), pp. 977–.

[32] Shia-Yen Teh, Robert Lin, Lung-Hsin Hung, and Abraham P. Lee, *Droplet microfluidics*, Lab Chip, 8 (2008), pp. 198–220.

[33] Sumita Pennathur Thomas M. Wynne, Alexander H. Dixon, *Electrokinetic characterization of individual nanoparticles in nanofluidic channels*, Microfluidics and Nanofluidics, 12 (2012), pp. 411–421.

[34] W. D. Volkmuth, T. Duke, M. C. Wu, R. H. Austin, and Attila Szabo, *Dna electrodiffusion in a 2d array of posts*, Phys. Rev. Lett., 72 (1994), pp. 2117–2120.

[35] John D. Weeks, David Chandler, and Hans C. Andersen, *Role of repulsive forces in determining the equilibrium structure of simple liquids*, J. Chem. Phys., 54 (1971), pp. 5237–5247.

[36] Hugo Wioland, Francis G. Woodhouse, Jrn Dunkel, John O. Kessler, and Raymond E. Goldstein, *Confinement stabilizes a bacterial suspension into a spiral vortex*, Phys. Rev. Lett., 110 (2013), pp. 268102–.